Perturbation analysis of the *Heterogeneous Quasi 1-D model* - a theoretical framework for predicting frequency response of AP-HTPB composite solid propellants

Vishal Wadhai[a], S. Varunkumar[a]

[a]Department of Mechanical Engineering, Indian Institute of Technology, Madras, Chennai 600 036, India

ARTICLE HISTORY
Compiled May 13, 2020

ABSTRACT
In this paper, the *Heterogeneous Quasi 1-D* model for steady combustion of AP-HTPB propellants is extended to the unsteady regime. The extended model is used to calculate the pressure-coupled frequency response (R_p) of low-smoke (non-aluminized) multi-modal AP-HTPB propellants. The R_p of a multi-modal propellant is expressed in terms of that of the individual *binder-matrix coated AP particles* constituting the statistical particle path. The weighting function, as expected from the *serial burning approach*, is the burn-time of particles. A closed-form expression is derived for the R_p of the particles by perturbation analysis of the quasi 1-D burn rate model. In this equation, all except the two parameters that quantify the amplitude (A_c) and phase (ϕ_c) of fluctuating heat flux on the solid side of the interface, are shown to be from the steady state model. This result establishes a strong connection between the steady and unsteady framework as compared to earlier models, where $R_p \to n$ (propellant pressure index) as $f \to 0$ was explicitly imposed. The model is used to predict R_p for a few low-smoke compositions. Effects of AP particle size distribution, mean pressure and initial temperature are brought out. When expressed as R_p/n vs f_s (non-dimensional frequency based on conduction time scale), the peak response magnitude is of $\mathcal{O}(1)$ and occurs close to non-dimensional frequency ($f_s = f\alpha/\bar{r}^2$) value of 1. While this conclusion is in line with the earlier results, it does not explain the ubiquitous nature of acoustic instability in tactical missile rockets, which requires the peak response to be at least an order of magnitude higher than n. Burn rate oscillations associated with the binder-melt effect caused by inhibitors is brought out as the most likely mechanism for the observed instabilities. Methods to extend the theory to include this effect is outlined.

KEYWORDS
AP-HTPB composite propellants; frequency response; serial burning; modeling; pressure coupling;

1. Introduction

AP-HTPB composite propellants with little or no aluminium are preferred in tactical solid rocket motors (SRMs) to avoid primary smoke. Solid rocket motors (SRMs) using such low-smoke compositions commonly encounter longitudinal mode acoustic instability leading to significant delays and loss of resources during development. Typical unstable behavior in such SRMs consists of the initial exponential growth of acoustic oscillations followed almost always by DC shift. DC shift is a sudden increase in

CONTACT S Varunkumar. Email: varuns@iitm.ac.in

the mean chamber pressure combined with very high amplitude (20-30% of mean) oscillations (see [1, 2]).

It is not uncommon to see the cause of instability being attributed to the absence of particulate damping associated with condensed Al/Al_2O_3 particles in the port. As shown in [2] the size range of Al/Al_2O_3 particles in the port can only affect waves of frequencies much higher (few thousand Hz) than what is encountered in longitudinal mode instabilities (a few hundred Hz).

It is important to note that relatively small amplitude limit cycle oscillations observed in long (>10 m) segmented motors are vortex shedding driven; oscillations in ARIANE 5 P230 booster is a case in point ([3]). This is due to the close to quasi-static pressure coupled response of the propellant to low frequency longitudinal standing modes (< 100 Hz). Unlike this, the instability in tactical SRMs are driven by the unsteady propellant combustion process and therefore can be explained only by recognizing the strong coupling between propellant combustion and port acoustics.

1.1. Pressure coupled response

Pressure coupling is quantified using *frequency response* (R_p). It is defined as the ratio of percentage fluctuation in mass burn rate of propellant to that of pressure. First phenomenological models for unsteady combustion of energetic solids were developed in the 1940s (see [4, 5]). In these 1-D models, the source of unsteadiness is due to transient heat conduction in condensed phase (gas phase assumed quasi-steady). These models were focused more towards homogeneous propellants.

Extensive work on unsteady propellant combustion modeling has been done in the US as well. The following assumptions are commonly used - (1) one dimensional homogeneous solid phase, (2) no reaction in the condensed phase, (3) Arrhenius type surface pyrolysis law and (4) quasi-steady gas phase. Referred to as the QSHOD models, all of these result in similar expressions for R_p as shown in [6] and is given by Equation 1.

$$R_p = \frac{m_s'/\bar{m}}{p'/\bar{p}} = \frac{AB}{\lambda + (A/\lambda) - (1+A) + AB}; \quad A = \frac{E_s}{R_0}\left(\frac{\bar{T}_s - T_i}{\bar{T}_s^2}\right) \tag{1}$$

where, A is related to the surface pyrolysis activation energy and B represents the gas phase response to pressure fluctuations. The specific form of B depends on the type of gas phase model chosen. A detailed description of forms taken by B under various gas phase model assumptions, including some cases where the quasi-steady assumption is relaxed can be found in [6]. Limitations of the QSHOD models when applied to heterogeneous composite propellants are clearly brought out in [6] and two relevant observations are reproduced below -

(1) The inadequacy of planar flame description without lateral diffusion in understanding unsteady combustion of composite propellants.
(2) The difficulties in obtaining large frequency response values (~ 3) without having to resort to unrealistically large values for the parameter A and/or including pressure dependence in surface pyrolysis law.

These limitations restrict the connection between QSHOD models and steady state propellant combustion to the imposed condition, $R_p \to n$ as $f \to 0$.

Multi-modal AP-HTPB propellants are heterogeneous solids. Attempts to couple QSHOD approach to simple steady models, like BDP and BDP based petite ensemble model (see [7, 8]) are reported in [9, 10]. The results obtained from these studies

have limitations due to assumptions inherent in the steady state models in accounting for heterogeneity (see [11]). These limitations of QHSOD-based models led to the development of 3D propellant pack CFD simulation models (see [12–14]). This elegant approach accurately accounts for the heterogeneity of the solid phase and its effect on the gas phase combustion. But it is computationally very expensive and therefore cannot be considered as a candidate design tool for practitioners. Also, it is not straightforward to account for the physical and chemical effects of several new additives (catalysts, inhibitors, energetic substances like nitramines) of interest to propellant designers in a CFD-based model.

1.2. The HeQu1-D model

A middle ground is sought in the current work. The result of which is a model which in simplicity matches the earlier generation models and in accuracy matches the CFD-based models in accounting for heterogeneity and lateral diffusion. These novel features of the *HeQu1-D model* has already been shown to be critical for accurately predicting steady deflagration rates of AP-HTPB propellants. Current work extends the steady state model to the unsteady regime. Details of the steady state model can be found in [15–17].

In the current work, the R_p of a multi-modal propellant is expressed in terms of that of the individual *binder-matrix coated AP particles* constituting the statistical particle path. Using linear perturbation analysis, a closed form expression is obtained for the frequency response of binder-matrix coated AP particles. Then, the R_p for two low smoke multi-modal AP-HTPB propellants are calculated. The results are used to bring out the effects of mean pressure, initial temperature, and most importantly the AP particle size distribution (PSD) on R_p. The inherent heterogeneity of wide-distribution AP propellants is shown to be accurately accounted for by this approach.

The peak response magnitude calculated using the model are, as expected, of the same order as the burn rate pressure index, n. This is consistent with the fact that low-smoke compositions with only AP and HTPB are *well behaved* (see [18]). Burn rate index of high solid loading ($> 84\%$) AP-HTPB only propellants is typically in the range of 0.4-0.6 and depends only on the AP particle size distribution. Hence the frequency response is usually less than 1, which is a strong indicator of stable combustion. Catalysts (iron oxide, activated copper chromate etc.) enhance the burn rate with little or no change in index (see [17]) and the frequency response.

1.3. Acoustic instability in tactical SRMs

Typical tactical SRMs have a length in the range of 1-4 m and operate in the pressure range of 70-150 atm. For a typical tactical SRM (2 m long and operating at 100 atm), results reported in [19, 20] show that the R_p must be at least 3 (in the frequency range of 100-1000 Hz) for the system to be linearly unstable. This observation is consistent with that reported in [6]. Also recall, as indicated in [6], that unusually large values of parameter A (the surface pyrolysis parameter in QSHOD models) are required to obtain such large response magnitudes which are inconsistent with the model parameters used for steady deflagration.

Another important conclusion from the results in [19, 20] is that the transition to DC shift is caused by cyclic de-pressurization–pressurization triggered extinction–re-ignition; a critical de-pressurization rate of about 8 atm/ms is shown to be required

to explain the typically observed shift in mean from about 120 atm to 180 atm. This critical de-pressurization rate is well below that of conventional AP-HTPB propellants (which is at least around 20 atm/ms at 120 atm).

All these factors point to the role of burn rate inhibitors (like strontium carbonate, titanium di-oxide etc.) as the primary factor responsible for instability. These additives are used in tactical missile rocket propellants to lower the burn rates as well as the pressure index. This effect, as shown in [15], is caused by binder-melt caused shielding of active AP surfaces; this leads to lowering of the burn rates of compositions with inhibitors to values less than that of pure-AP. This can occur at pressures as low as 50 atm (termed *crossover pressure*). This effect was incorporated into the *HeQu1-D model* by introducing the binder-melt effect through the f_{ll} term; this term denotes the fraction of AP surface shielded by binder-melt. The f_{ll} factor was taken to be a function of the *transfer number* (B) and modeled as an extreme case of boundary layer *blocking effect* similar to what is observed in hybrid rockets.

This shielding effect of active AP surfaces can also explain the lower critical de-pressurization rates of propellants with inhibitors as compared to conventional propellants. Given that the burn rates of the compositions with inhibitors become lower than that of pure-AP at pressures as low as 50 atm, the critical dp/dt for these compositions can even be lower than that of pure-AP (which is less than 10 atm/ms). This is consistent with the observations in [19, 20].

In the current work, dynamic fluctuations in the binder-melt is hypothesized to be the cause for high R_p of propellants with inhibitors. By extending the steady binder-melt model to include additional burn rate fluctuations due to dynamic binder-melt fluctuations, a framework to explain the high response function values is presented. A methodology is outlined to incorporate this effect into the analytical framework developed here and representative results are presented.

2. Unsteady *HeQu1-D* model

First the serial burning *statistical particle path* description is extended to the unsteady regime by perturbation analysis. Following this, the perturbation analysis of the burn rate model for the binder-matrix coated AP particle is presented. Aspects of the *HeQu1-D* model are introduced and discussed briefly whenever required. More details of the steady state model are available in [15–17].

2.1. Statistical particle path

In the serial burning approach, the burn rate, $\dot{r}$, of a composite solid propellant containing AP particles of diameters d_1, d_2, ..., d_n and corresponding mass fractions of f_1, f_2, ..., f_n is calculated using Equation 2.

$$\dot{r}(p) = \left[\sum_i \frac{l_i}{\dot{r}_i(p)} \right]^{-1} \tag{2}$$

where, p is pressure, l_i and $\dot{r}_i$ are the line average intersection and burn rate of binder-matrix coated AP particle of diameter d_i. Introducing the decomposition,

$$\dot{r}_i = \bar{\dot{r}_i} + \dot{r}_i{}', \;\; \dot{r} = \bar{\dot{r}} + \dot{r}'$$

into Eqn. 2 leads to

$$\frac{1}{\bar{\dot{r}}+\dot{r}'} = \sum_i \frac{l_i}{\bar{\dot{r}}_i+\dot{r}_i{}'} \Rightarrow \frac{1}{1+\dot{r}'/\bar{\dot{r}}} = \bar{\dot{r}}\sum_i \frac{l_i}{\bar{\dot{r}}_i}\frac{1}{1+\dot{r}_i{}'/\bar{\dot{r}}_i}$$

Linearising this equation results in,

$$1-\frac{\dot{r}'}{\bar{\dot{r}}} = \bar{\dot{r}}\sum_i \frac{l_i}{\bar{\dot{r}}_i} - \bar{\dot{r}}\sum_i \frac{l_i}{\bar{\dot{r}}_i}\frac{\dot{r}_i{}'}{\bar{\dot{r}}_i} = 1-\bar{\dot{r}}\sum_i \frac{l_i}{\bar{\dot{r}}_i}\frac{\dot{r}_i{}'}{\bar{\dot{r}}_i},$$

since $\sum_i l_i = 1$. Dividing both sides by $p'/\bar{p}$ gives Eqn. 3, which is the propellant response in terms of response of binder-matrix coated AP particles. Note that the weighting function is the burn time of binder-matrix coated AP particles ($l_i/\dot{r}_i$).

$$R_p = \frac{\dot{r}'/\bar{\dot{r}}}{p'/\bar{p}} = \bar{\dot{r}}\sum_i \frac{l_i}{\bar{\dot{r}}_i}R_{p,i} \tag{3}$$

$$R_{p,i} = |R_{p,i}|\, e^{i\phi_{p,i}} = \frac{\dot{r}_i{}'/\bar{\dot{r}}_i}{p'/\bar{p}}; \quad \phi_{p,i} = cos^{-1}\left(\frac{< r_i', p' >}{\sqrt{< r_i', r_i' >< p', p' >}}\right) \tag{4}$$

where, $\bar{\dot{r}}$ and $\bar{\dot{r}}_i$ represent the propellant and individual particle burn rates under the steady conditions respectively, and are obtained using the *HeQu1-D* model. Note the similarities between Eqn. 3 obtained for frequency response of the propellant and that of the steady pressure index given by Eqn. 5.

$$n = \bar{\dot{r}}\sum_i \frac{l_i}{\bar{\dot{r}}_i}n_i; \quad n_i = \left(\frac{\partial r_i}{\partial p}\right)_{\bar{p}} \tag{5}$$

At zero frequency, when frequency response of the individual particles ($R_{p,i}$) tend to index of the particles (n_i), the condition of $R_p = n$ is automatically satisfied.

The R_p is a complex number; the magnitude ($|R_{p,i}|$) represents the amplitude of burn rate fluctuations relative to the imposed pressure fluctuations and the angle (ϕ_p) represents the phase difference between burn rate and pressure fluctuations (Equation 4). The time domain counterpart of frequency response is called the *burn rate impulse function*.

2.2. Perturbation analysis of the surface heat balance equation

Surface heat flux balance for a binder-matrix coated AP particle is given by Equation 6.

$$k\left[\frac{dT}{dx}\right]_{0^-} = \rho_p \dot{r} H_s + k\left[\frac{dT}{dx}\right]_{0^+} \tag{6}$$

where, LHS represents the heat flux from surface into the condensed phase ($\dot{q}_c$), the first term on RHS represents the enthalpy change associated with solid to gas phase transformation at the interface (ρ_p is the density of condensed phase, H_s is the enthalpy

change per unit mass of solid to gas transformation) and the second term on RHS represents the heat flux from the gas phase flame to the surface ($\dot{q}_g$).

It is convenient for the algebraic transformations for the perturbation analysis of surface heat flux balance to treat the surface temperature as the primary variable. This is easier due to the direct connection between the burn rate and the surface temperature through the Arrhenius pyrolysis law, $\dot{r} = A_s e^{-E_s/RT_s}$. This enables tabulation of the condensed phase heat flux fluctuations as a function of frequency (more details are given later). This approach has two advantages - first, the reduction in the computational effort and second and most importantly, closed-form expression can be obtained for the frequency response.

2.2.1. Condensed phase

For an imposed sinusoidal fluctuation in surface temperature,

$$T_s = \bar{T_s}(1 + \epsilon_T sin(2\pi f t))$$

the fluctuation in the condensed phase heat flux can be expressed as,

$$\dot{q}_c = \bar{\dot{q}_c}(1 + A_c \epsilon_T sin(2\pi f t + \phi_c)) \tag{7}$$

where, ϵ_T is the amplitude and f is the frequency of the fluctuation in T_s, A_c is the flux amplification factor, ϕ_c is the phase difference between T_s and $\dot{q}_c$ and t represents time. Quantities with an over-bar represent steady state values. The condensed phase heat flux under steady condition is $\bar{\dot{q}_c} = \rho_p \bar{\dot{r}} c_p (\bar{T_s} - T_0)$. Quantities A_c and ϕ_c are obtained by numerical solution of transient heat conduction equation in the solid phase; details of coordinate transformation used to map the semi-infinite domain to a finite domain and numerical solution procedure are outlined in Appendix.

2.2.2. Gas phase

Gas phase heat flux, $\dot{q}_g$ for a binder-matrix coated AP particle is given by Equation 8.

$$\dot{q}_g = \frac{\rho_p \dot{r}_i c_p (T_{eff} - T_s) g_f}{\xi^*_{eff} - 1} \tag{8}$$

where, $g_f = (d_i/(d_i + 2t_{bm}))^2$ is the geometric factor to account for effective heat transfer area, T_{eff} is an effective flame temperature and ξ^*_{eff} is an effective non-dimensional flame stand-off distance. Effective non-dimensional flame stand-off distance is given by Equation 9, where x^*_{eff} is effective flame stand-off distance which can be obtained from mass flux balance at the propellant surface; $K_{r,eff}$ is the effective gas phase reaction rate constant.

$$\xi^*_{eff} = exp\left(\frac{\rho_p \dot{r} c_p x^*_{eff}}{k_g}\right); \quad \rho_p \dot{r} = K_{r,eff} p^2 x^*_{eff}; \quad K_{r,eff} = A_g exp\left(-\frac{E_g}{RT_{eff}}\right) \tag{9}$$

Effective flame temperature, T_{eff}, depends on the extent of lateral diffusion of AP and binder decomposition products into each other. Two limiting cases, namely, AP mono propellant which burns with flame temperature of 1250 K [21, 22] and premixed binder-matrix whose flame temperature depends on the O/F ratio, are used to obtain

T_{eff} of a particle (Equation 10).

$$\frac{T_{eff} - 1250}{T_{f,ad} - 1250} = \frac{1 - e^{-z}}{z}; \quad z = \frac{d_{AP}}{d_o} \tag{10}$$

where, z is a nondimensional distance defined as the ratio of AP diameter to a diffusion distance (d_0).

In the Equation 10, effective flame stand-off distance (T_{eff}) depends on the diffusion distance (d_o) which quantifies the extent of diffusion of decomposition products. Diffusion distance (d_o) is the reaction limited diffusion length scale given by Equation 11.

$$d_0 = d_{0,ref}(1 - \phi)\left(\frac{20}{p}\right)\sqrt{\frac{30000}{K_r}} \tag{11}$$

As suggested in [15], $d_{o,ref} = 90$ μm is used here also. The non-dimensional variable z is related to the Damkohler number through, $z = \sqrt{Da}$.

Surface enthalpy change (H_s) for composite propellant is taken as the mass fraction weighted average of the component enthalpies. For AP-HTPB based composite propellants, H_s is given by,

$$H_s = f_{AP}H_{AP} + H_{bm}; \quad H_{bm} = \sum_i f_i H_i \tag{12}$$

where H_{bm} is enthalpy of binder-matrix (composed of HTPB, extinct and fine AP) and given by

$$H_{bm} = f_{HTPB}H_{HTPB} + (f_{pm} + f_{ex})H_{AP}$$

Perturbation of Equation 8 leads to Equation 13.

$$\dot{q}_g = \bar{\dot{q}}_g\left[1 + \left[1 - \frac{\theta_{fs,eff}}{e_s} - 2g(B_{eff})\right]\frac{\dot{r}_i'}{\bar{\dot{r}}_i} + \left[z_r\frac{\bar{T}_{eff}}{\bar{T}_{eff} - \bar{T}_s} + g(B_{eff})e_g z_r + 2g(B_{eff})\right]\frac{p'}{\bar{p}}\right] \tag{13}$$

where,

$$\theta_{fs,eff} = \frac{\bar{T}_s}{\bar{T}_{eff} - \bar{T}_s}; \quad B_{eff} = \frac{\bar{T}_{eff} - \bar{T}_s}{\bar{T}_s - T_s - H_s/c_p}; \quad z_r = \frac{(T_{f,ad} - 1250)}{\bar{T}_{eff}}\left[\frac{e^{-\bar{z}}(1+\bar{z}) - 1}{\bar{z}}\right] \tag{14}$$

$$e_g = \frac{E_g}{R\bar{T}_{eff}}; \quad g(B_{eff}) = \frac{(1 + B_{eff})\ln(1 + B_{eff})}{B_{eff}} \tag{15}$$

The expressions for the fluctuating gas phase heat (Equation 13) and condensed phase (Equation 7) are substituted in Equation 6 to get an expression for $R_{p,i}$ for binder-matrix coated AP particle (Equation 16).

$$R_{p,i} = \frac{2 + h_s/(1-h_s)(0.6 f_{AP}\bar{p})/(g_f\bar{H}_s)(1/g(B_{eff})) + z_r[e_g + (1/g(B_{eff}))\bar{T}_{eff}/(\bar{T}_{eff} - \bar{T}_s)]}{2 + (g_f\theta_{fs,eff}(1-h_s) + A_c cos(\phi_c) - e_s h_s - g_f e_s(1-h_s))/(g_f g(B_{eff})(1-h_s)e_s)} \tag{16}$$

Equation 16 for $R_{p,i}$ of binder-matrix coated AP particle reduces to Equation 17 for pure-AP and homogeneous propellant (that is for fine-AP-HTPB mixtures) because of the absence of lateral-diffusion.

$$R_{p,premixed} = \frac{2 + h_s/(1-h_s)(0.6\bar{p})/\bar{H}_s(1/g(B))}{2 + (\theta_{fs}(1-h_s) + A_c\cos\phi_c - e_s)/(g(B)(1-h_s)e_s)} \tag{17}$$

Term-by-term comparison of $R_{p,premixed}$ and $R_{p,i}$ is given in Table 1. The additional term t_2 in the expression of $R_{p,i}$ accounts for the effect of lateral diffusion and all other terms are same as that in $R_{p,premixed}$ but with modified parameters.

Table 1. Comparison of the terms in the expression of magnitude of frequency response of premixed limit and binder-matrix coated AP particle.

$R_p = \frac{2+t_1+t_2}{2+t_3}$	$R_{p,premixed}$	$R_{p,i}$
t_1	$\frac{0.6\bar{p}h_s/(1-h_s)}{\bar{H}_s g(B)}$	$\frac{0.6\bar{p}h_s/(1-h_s)}{\bar{H}_s g(B_{eff})}$
t_2	-	$z_r[e_g + \bar{T}_{eff}/(g(B_{eff})(\bar{T}_{eff} - \bar{T}_s))]$
t_3	$\frac{\theta_{fs}(1-h_s)+A_c\cos\phi_c-e_s}{g(B)(1-h_s)e_s}$	$\frac{\theta_{fs,eff}(1-h_s)+A_c cos(\phi_c)-e_s}{g(B_{eff})(1-h_s)e_s}$

3. Results and discussion

3.1. Frequency response for pure AP and binder-matrix

The magnitude of frequency response for the premixed limits is calculated using Equation 17. Steady state parameters required for calculating R_p, obtained from the HeQu1-D model, are given in Table 2. The product, $A_c\cos\phi$, is the only frequency dependent parameter which enters the expression for R_p (see Eqn. 17) and is shown in Fig. 1 for pure AP at $\bar{T}_s$ values corressponding to 20.7, 68.9 and 120 atm.

The temperature profile in condensed phase responds to any boundary changes with the time scale of the order of $\alpha/\bar{r}^2$. Minimum amplification is obtained at f_s close to 1 as shown in Figure 1. This implies that a minimum change in heat flux is required to obtain a given change in surface temperature when both changes take place at same time scale. In Figure 1, it can be seen that the term $A_c cos\phi_c$ decreases with increase in mean surface temperature at all frequencies.

The frequency responses for pure AP and homogeneous propellant (AP/HTPB - 86% /14%) at pressures of 20.7, 68.9 and 120 atm at an initial temperature of 300 K are shown in Figures 2a and 2b, respectively. The frequency response is shown in the form of ratio of magnitude of frequency response to pressure index, $|R_p|/n$ and the phase difference, ϕ_p.

The magnitude of frequency response of pure AP, as well as homogeneous propellant, decreases with increase in pressure. This is directly related to flame stand-off distance being an inverse function of pressure (Equation 9); since the rate of decrease of x^* decreases with increase in mean pressure, the corresponding burn rate fluctuations

Table 2. Steady state combustion parameters of pure AP and homogeneous AP-HTPB calculated using *HeQu1-D* model [15, 16].

Parameters	AP			Binder-matrix (86/14–AP/HTPB)		
	20.7 atm	68.9 atm	120 atm	20.7 atm	68.9 atm	120 atm
$\bar{T_s}$, (K)	873	994	1057	1131	1386	1540
T_f (K)	1250	1250	1250	2862	2862	2862
$\bar{H_s}$ (kJ/kg)	460	487	515	312	334	359
B	3.3	1.2	0.8	3.3	2.0	1.5
h_s	0.80	0.70	0.67	0.37	0.30	0.28
$g(B)$	1.90	1.45	1.32	1.90	1.64	1.52
θ_{fs}	2.3	3.9	5.5	0.7	0.9	1.2
n	0.75	0.73	0.72	0.86	0.86	0.85

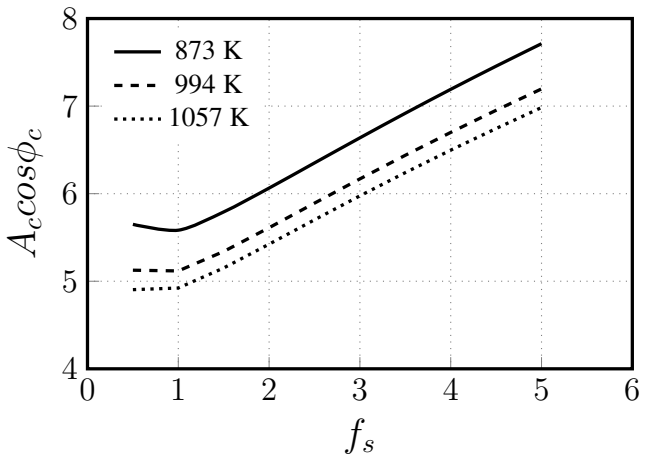

Figure 1. Effect of mean pressure (mean surface temperature) on $A_c \cos\phi$ for pure AP

also decrease leading to lower R_p at higher pressures.

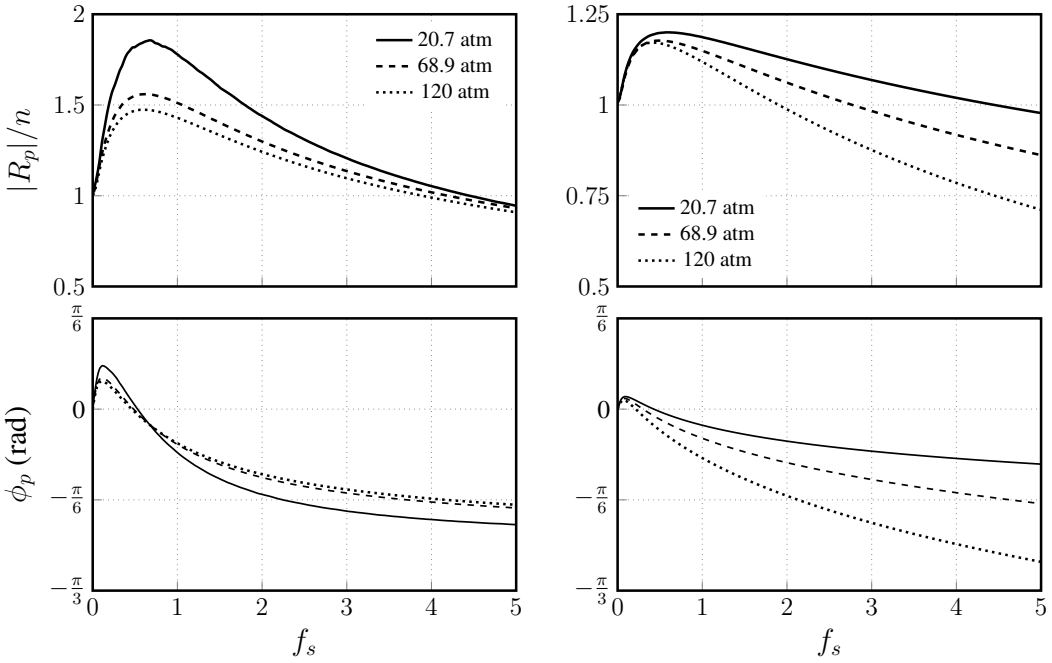

(a) Pure AP (b) 86/14–AP/HTPB binder-matrix

Figure 2. Premixed limit pressure coupled frequency responses at an initial temperature of 300 K for different mean pressures.

3.2. Frequency response of AP/HTPB propellants

Two high energy (87.4% AP loading) multi-modal AP-HTPB propellants, namely, SD-III-18 and SD-III-21, were chosen for analysis from [23]. The choice of propellants is based on the following two considerations - (1) availability of steady burn rate data and (2) detailed AP particle size distribution. The predicted steady propellant burn rates for above mentioned propellants are shown in Table 3. The predicted steady state burn rates are within ± 3% of experimental results for SD-III-18 and within 20% for SD-III-21. The larger deviation with SD-III-21 is believed to be due to issues in experimental data. This is inferred from the fact that the burn rate of SD-III-21 at 68.9 atm is 8.4 mm/s, which is the same as that of pure-AP at 68.9 atm. A high energy composition with no additives is expected to burn at rates higher than pure-AP. Recall that the response function calculation using the unsteady model requires a number of parameters from the steady model and therefore the steady model must be capable of accurately predicting the burn rate and pressure index.

Table 3. Composition details and predicted steady state results for conventional propellants from [23].

Propellant	Composition		Burn rate (mm/s)		
	Particle size (μm)	Fraction (%)	20.7 atm	68.9 atm	120 atm
SD-III-18	90/20	42.12/45.28	10.5 (10.2)	18.0 (18.2)	22.9 (-)
SD-III-21	400/200/50/20	31.6/31.6/10.52/13.69	6.2 (5.0)	10.0 (8.4)	13.8 (-)

Predicted values of the magnitude and the phase of R_p for SD-III-18 and SD-III-21

at three pressures, 20.7, 68.9 and 120 atm are shown in Figure 3.

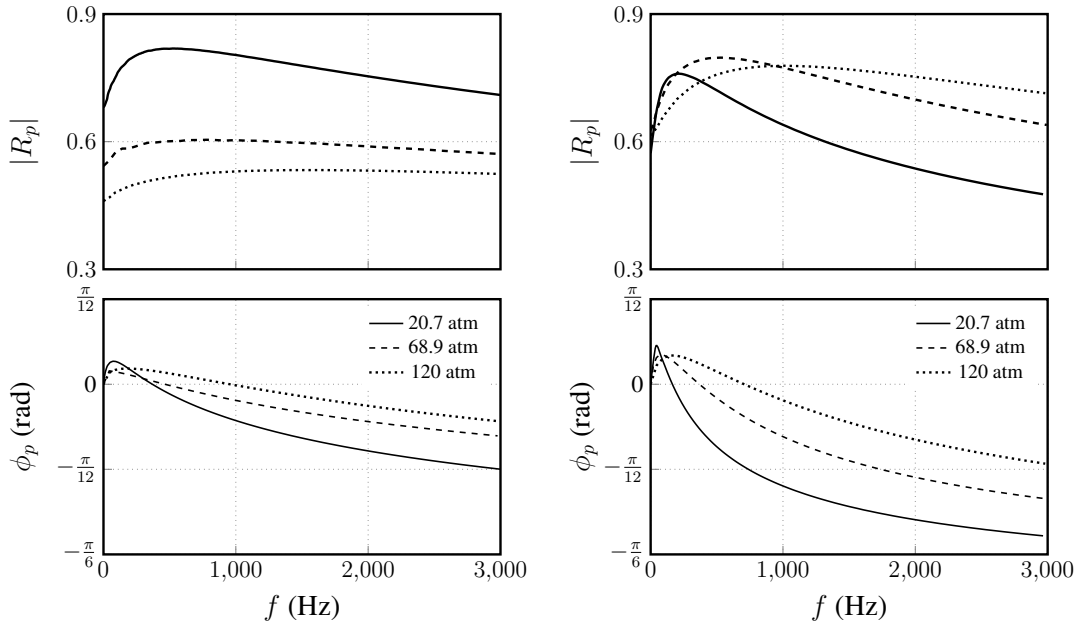

(a) SD-III-18 (b) SD-III-21

Figure 3. Frequency response showing $|R_p|$ and ϕ_p vs dimensional frequency, f for propellants SD-III-18 and SD-III-21

Effect of mean pressure

Unlike that of pure-AP and binder-matrix, the peak frequency response of a multi-modal AP-HTPB propellant does not always decrease with increase in pressure. Propellant SD-III-21 is a case in point - the magnitude of peak response increases with pressure from 20.7 to 68.9 atm and then decreases. Also, for SD-III-21, the magnitude of frequency response at frequencies higher than peak frequency increases as mean pressure increases from 68.9 to 120 atm. Experimental results reported in [24] for similar compositions are consistent with these observations.

This behavior is because of the following - the overall response of the composite propellant depends on that of binder-matrix coated AP particles (Equation 16). Unlike in the case of pure-AP and homogeneous propellants, the effective temperature (T_{eff}) of binder-matrix coated AP particle varies with pressure and O/F (T_{eff} is dependent on $z = d_{AP}/d_0$ and d_0 is inversely proportional to pressure). Therefore with increase in pressure, the deflagration of coated AP particles shift towards mono-propellant limit. This, depending on the particle size and O/F can lead to an increase or decrease in response (see Figure 4). Therefore accounting for the heterogeneity due to multi-modal AP distribution is critical to capture the pressure dependence of frequency response.

Calculated frequency response at 250 Hz for 25, 100 and 400 μm particles with three different O/F ratios is shown in Figure 4. For particles controlled predominantly by premixed flames (25 μm with 78 and 87.43% AP and 400 μm with 99.24% AP), the R_p decreases with increase in pressure as expected. For other cases, the R_p magnitude is a complex function of pressure and the extent of lateral diffusion.

Figure 5 shows the variation of scaled response (R_p/n) with non-dimensional fre-

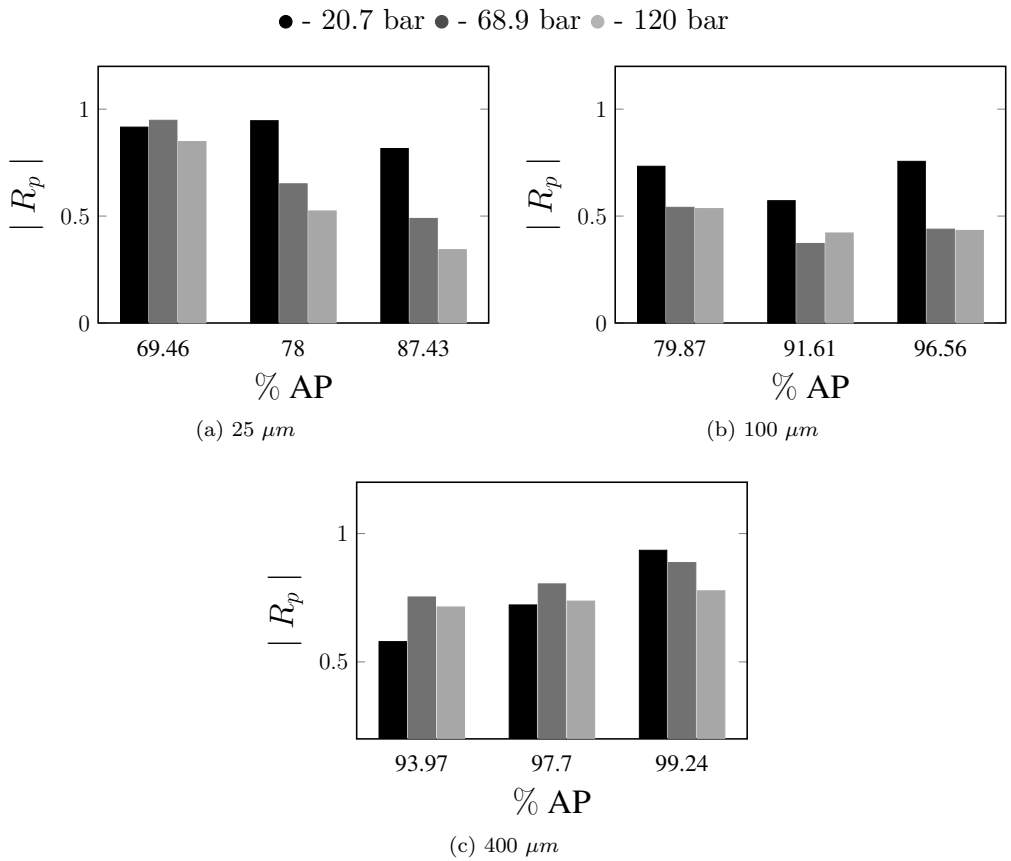

Figure 4. Mean pressure effect on frequency response of AP particle of different sizes and O/F at 250 Hz.

quency, $f_s = f\alpha/\bar{\dot{r}}^2$. As expected, peak values of R_p is of the same order as n. Note that, unlike in the case of pure-AP and homogenized AP/HTPB mixtures, the peak R_p is not exactly at $f_s \sim 1$; this is due to the fact that the propellant mean burn rate is used for calculating f_s, while the response function magnitude is dependent on the contribution of particles of different sizes. That the peak occurs at $f_s < 1$, indicates to the greater influence of faster burning particles as compared to larger particles. These are expected to be general features of the variation of R_p with f for multi-modal AP-HTPB propellants.

3.2.1. Effect of initial temperature

Frequency response corresponding to initial temperatures of 240, 300 and 340 K at a pressure of 68.9 atm are given in Figure 6 for SD-III-18 and SD-III-21. It shows a slight decrease in frequency response with an increase in the initial temperature. The unsteady behaviour of composite propellant with respect to the initial temperature of condensed phase is expected to be same as that of pure AP as the condensed phase is modelled similarly to pure AP.

A detailed discussion of the effects of AP particle size distribution, solid loading and catalysts is presented in [20]. The analysis is based on the R_p predicted for several AP-HTPB-catalyst propellants. Given that the general conclusion for these propellants is that the $R_p/n \sim 1$ and therefore SRMs using these compositions are expected to be stable, the details are not included here (see [20] for a detailed discussion). But the

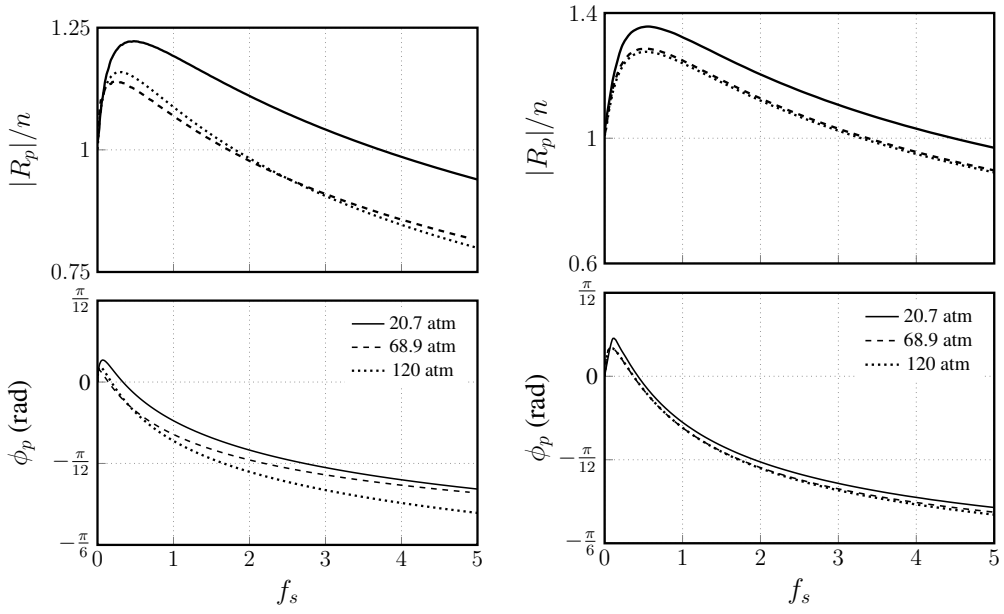

(a) SD-III-18 (b) SD-III-21

Figure 5. Frequency response showing $|R_p|/n$ and ϕ_p vs non-dimensional frequency, f_s for propellants SD-III-18 and SD-III-21

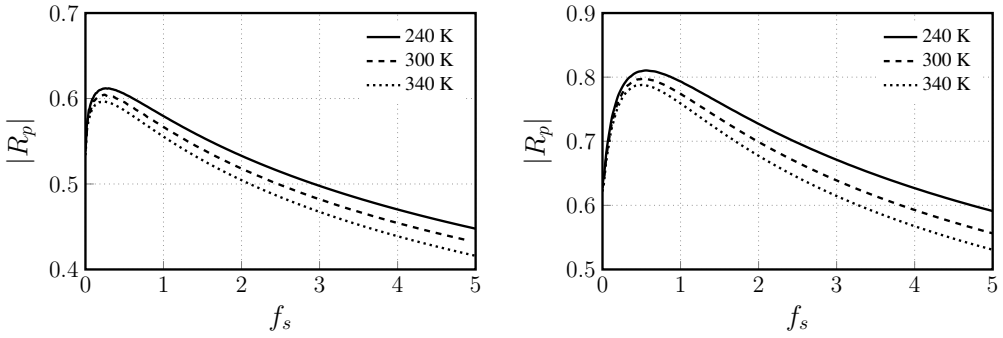

(a) SD-III-18 (b) SD-III-21

Figure 6. Effect of initial temperature on frequency response of propellants SD-III-18 and SD-III-21 at pressure of 68.9 atm.

question, *what causes the peak propellant response to be as high as ten times the index* (required for instability) remains still unanswered. A possible scenario leading to high response is outlined in the following section.

4. Effect of burn rate inhibitors

In practice, high energy (>80% AP) and low index ($n < 0.3$) compositions are sought. Note that adding aluminum is not an option for low-smoke applications. But the minimum index achievable with only AP and HTPB is 0.4 ([15]). Therefore, in practice $n < 0.3$ can only be achieved with special burn rate suppressing additives. Common additives include strontium carbonate, oxamide and titanium di-oxide.

It is also generally believed that low pressure index is beneficial for dynamic stability. This does not seem to be the case, as the mechanism responsible for reduction of burn rate and pressure index in the presence of inhibitors also significantly increases the heterogeneity of the surface. Consider two compositions of similar total energy without and with inhibitors. The one without the inhibitor will have a burn rate index of at least 0.4. On the other hand, the one with the inhibitor will have an index lower than 0.3. As shown in [15], this reduction in index is brought about by the binder melt caused by inhibitors. Through endothermic decomposition at the surface, inhibitors prevent the gasification of HTPB leading to lateral spread of binder-melt over active AP surfaces. The effect of binder-melt under steady conditions is explained in [15] using an extension of the blocking effect.

Frequency response calculated assuming quasi-static binder-melt fluctuation is shown in Figure 7. The results indicate clearly that the quasi-static assumption is not valid as the predicted R_p is still of order n.

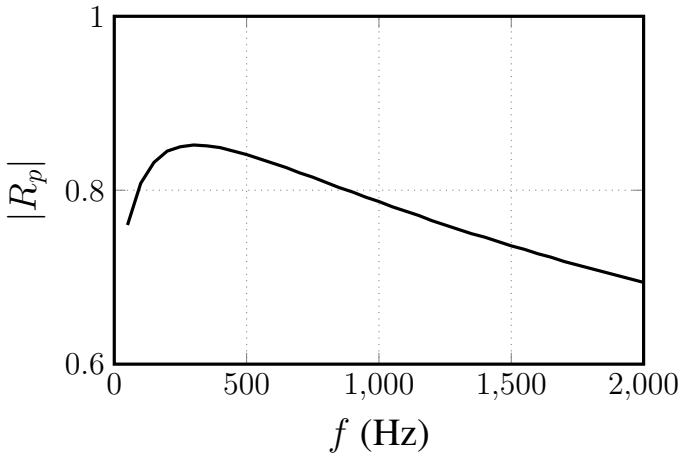

Figure 7. Frequency response for COM1 at pressure of 68.9 atm calculated without using extra dynamics.

Therefore, the binder-melt must be dynamically responding to pressure fluctuations. As brought out earlier, this is likely due to the enhanced heterogeneity in the surface decomposition enthalpy. These additional fluctuations in the area covered by binder melt can be accounted for by the introduction of $f_{ll}^{'}$ which is defined as,

$$\frac{f_{ll}^{'}(f)}{\bar{f}_{ll}} = -f_{ll,amp}\frac{p^{'}(f)}{\bar{p}} \tag{18}$$

With this, total area covered by liquid layer becomes $f_{ll} = \bar{f}_{ll} + f_{ll}^{'}$ which is obtained using calibrated value of $f_{ll,amp}$. The negative sign in Eqn. 18 indicates the out-of-phase relationship between the fluctuations in pressure and binder-melt; there will be a decrease in area covered by liquid layer as pressure starts to increase in a particular cycle of oscillation and vice-versa. This will result in an increase of the amplitude of burn rate oscillations and hence the frequency response.

By linearizing the governing equations in the limiting condition of decomposition of the inhibitor at the propellant surface, the expression for the R_p of binder-matrix

coated AP particle is obtained and is given in Equation 19.

$$R_{p,i} = \frac{2 + \frac{h_d}{1-h_d}\frac{c_1\bar{p}}{g(B_{eff})\bar{f}_{nll}(\bar{H}_s+f_{SC}H_d)} + z_r\left[e_g + \frac{1}{g(B_{eff})}\frac{\bar{T}_{eff}}{\bar{T}_{eff}-\bar{T}_s}\right] + f_{ll,amp}\frac{\bar{f}_{ll}}{\bar{f}_{nll}}}{2 + \frac{\bar{f}_{nll}\theta_{fs,eff}(1-h_d)+A_c sin(2\pi f_s\tau+\phi_c)-e_s h_d-\bar{f}_{nll}(1-h_d)e_s}{\bar{f}_{nll}g(B_{eff})(1-h_d)e_s}} \quad (19)$$

The expression for frequency response (Eqn. 19) includes a parameter $f_{ll,amp}$ which can be obtained, as of now, only by calibration with a known frequency response value. Calibrated frequency function of $f_{ll,amp}$ to obtain peak response of 3 at 250 Hz is shown in Figure 8a and the corresponding frequency response is shown in Figure 8b. Perhaps, experiments can be used to validate this approach. Frequency response for COM1 is dominated by frequency function of $f_{ll,amp}$ and it is dependent on the value of $\bar{f}_{ll}/\bar{f}_{nll}$ (Equation 19).

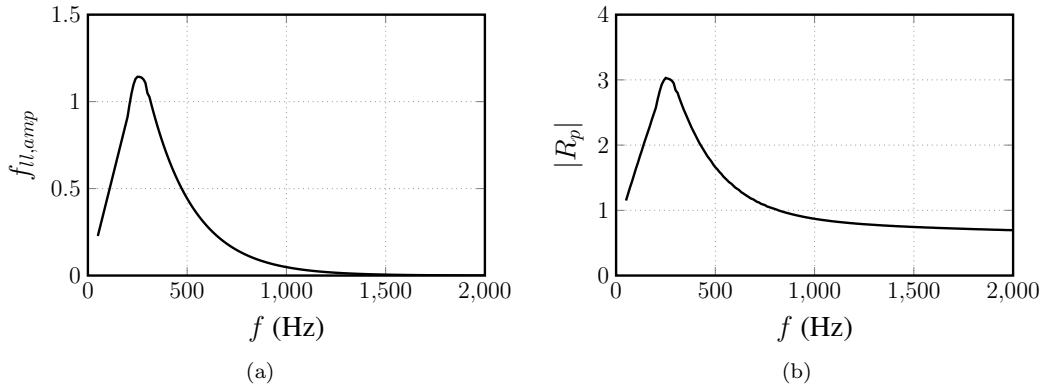

Figure 8. (a) Frequency function of $f_{ll,amp}$ (b) Frequency response for COM1 at pressure of 68.9 atm calculated using $f_{ll,amp}$.

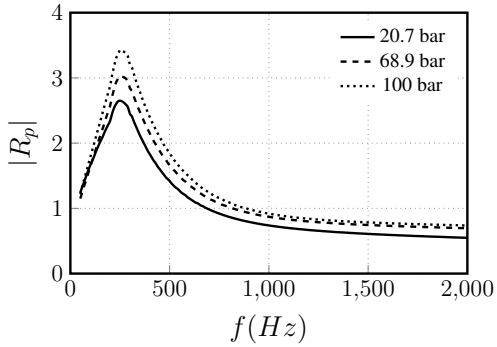

Figure 9. Frequency response for COM1 calculated using $f_{ll,amp}$ at pressures of 20.7 and 68.9 atm

Figures 9 shows the effect of mean pressure on the magnitude of frequency response. Unlike conventional propellants, R_p of COM1 increases with increase in mean pressure. This is because the ratio $\bar{f}_{ll}/\bar{f}_{nll}$ from the expression of frequency response (Equation 19) increases with increase in mean pressure. This result is a likely explanation for some conflicting observations on the pressure dependence of R_p found in literature. It is consistent with the fact that the SRMs are more prone to instability at higher pressure (beyond the effect of reduced damping at higher pressure).

5. Conclusions

The *HeQu1-D* framework for steady deflagration of AP-HTPB propellants was extended to unsteady regime using linear perturbation analysis. Analytical expressions were derived for frequency response of pure-AP, binder-matrix and binder-matrix coated AP particles. Consistency with steady state parameters was established – $R_p \to n$ as $f \to 0$ follows from the theory and not imposed. Notably, A_c and ϕ_c which appear in the expression of frequency response, are the only unsteady terms that enter the expression for R_p. Numerical procedure for calculating A_c and ϕ is described. Analysis of the behavior of conventional propellants (AP-HTPB only) under fluctuating pressure confirms the following well-known results from the literature: (1) the frequency response of conventional propellants is of the same order as the burn rate index, (2) in general, there is a marginal decrease in the magnitude of the peak frequency response with an increase in mean pressure and initial propellant temperature and (3) catalysts have no effect on this general behavior. Binder-melt modulated fluctuations in burn rate is hypothesized to be the cause of $R_p/n \sim \mathcal{O}(10)$. The important result brought out with current modeling of binder melt flow is the increase in frequency response with an increase in mean pressure. This is in contrast with the behavior of conventional propellant and is a likely explanation for some conflicting results for frequency response - mean pressure trend found in the literature. Indeed, in the absence of adequate experimental measurements, this was an attempt to model the additional fluctuations in heat flux feedback responsible for the increase in frequency response. Further experiments are needed to fully understand the complex dynamics of binder-melt flow over AP-HTPB composite propellants under static and dynamic conditions. Efforts in this direction are under way and are expected to transform the unsteady model to be a tool for propellant development for stable combustion.

Acknowledgments

Extensive discussions with Prof. H S Mukunda (IISc, Bangalore, retired) were instrumental in development of the theory and we thank him for his contributions.

Notation

A_c	Heat flux amplification factor
A_s	pre-exponential constant, mm/s
B	Transfer number
B_{eff}	effective transfer number
c_p	specific heat capacity, J/kg K
D	Diffusion constant, μm^2/s
d_0	Diffusion distance, μm
$d_{0,ref}$	Reference diffusion distance, μm
d_i	Diameter of AP particle, i, μm
E_s	Solid phase activation energy, J/kg
E_g	Gas phase energy of activation, J/kg
f	Frequency, Hz
f_{ex}	Burn rate modifier mass fraction
f_{ex}	Extinct AP particle mass fraction

f_{HTPB}	HTPB mass fraction
f_{pm}	AP mass fraction below premixed cutoff diameter
f_{ll}	Fraction of the surface covered by binder matrix
$f_{ll,amp}$	Amplitude of fluctuation in f_{ll}
f_{nll}	Fraction of the surface not covered by binder matrix
f_s	Non-dimensional frequency
g_f	Geometric factor
H_{AP}	Enthalpy change for AP at surface due to phase change, kJ/kg
H_{bm}	Enthalpy change for binder-matrix at surface due to phase change, kJ/kg
H_{HTPB}	Enthalpy change for HTPB at surface due to phase change, kJ/kg
H_s	Net enthalpy change at surface due to phase change, KJ/kg
k	Thermal conductivity, W/m K
k_g	Thermal conductivity of gas phase, W/m K
K_r	Gas phase reaction rate, s/m^2 atm
$K_{r,eff}$	Effective gas phase reaction rate, s/m^2 atm
l_i	Line average intersection of binder-matrix coated AP particle of diameter, d_i
n	pressure index
n_i	pressure index of binder-matrix coated AP particle of diameter, d_i
p	pressure, atm
$\dot{q}_c$	Solid phase heat flux rate, W/m^2 s
$\dot{q}_g$	Gas phase heat flux rate, W/m^2 s
R	Universal gas constant, J/mol-K
$\dot{r}$	Propellant burn rate, mm/s
$\dot{r}_i$	Burn rate of binder-matrix coated AP particle of diameter, d_i, mm/s
R_p	Pressure coupled frequency response
$R_{p,i}$	Pressure coupled frequency response of AP particle
T_0	Initial temperature of solid propellant, K
t_{bm}	Thickness of binder matrix, μm
T_{eff}	Effective flame temperature, K
T_f	Adiabatic flame temperature, K
$T_{f,ad}$	Adiabatic flame temperature of homogenised binder-matrix coated AP particle, K
T_s	Surface Temperature, K
V_i	Volume fraction
x^*	Flame stand off distance, μm
x^*_{eff}	Effective flame stand off distance, μm
α	Thermal diffusivity, m^2/s
ϵ_T	Amplitude of fluctuation in surface temperature
ϕ_c	Phase difference between q_c and T_s, rad
ϕ_p	Phase difference between $\dot{r}$ and p, rad
ϕ	Homogenised binder-matrix equivalence ratio
ρ_{brm}	Density of burn rate modifier, kg/m^3
ρ_{HTPB}	Density of HTPB, kg/m^3
ρ_{AP}	Density of AP, kg/m^3
ρ_p	Density of propellant, kg/m^3
τ	Non-dimensional time
ξ^*	Non-dimensional flame stand off distance
ξ^*_{eff}	Effective non-dimensional flame stand off distance

References

[1] F.S. Blomshield, *Historical perspective of combustion instability in motors: case studies*, AIAA Paper 3875 (2001), p. 2001.

[2] F.S. Blomshield, *Lessons learned in solid rocket combustion instability*, Defense Technical Information Center, 2006.

[3] F. Vuillot and G. Casalis, *Motor flow instabilities-part 1*, Tech. Rep. RTO-EN-023, ONERA-MEUDON CENTRE (FRANCE), 2004.

[4] Y.B. Zel'dovich, *On theory of burning of the gunpowder and explosives*, J. Exper. Theoret. Phys 12 (1942), pp. 498–524.

[5] B.V. Novozhilov, *Nonstationary combustion of solid rocket fuels*, Tech. Rep. FTD-MT-24-317-74, DTIC Document, 1973.

[6] F. Culick, *A review of calculations for unsteady burning of a solid propellant.*, AIAA Journal 6 (1968), pp. 2241–2255.

[7] M. Beckstead, *A model for solid propellant combustion*, in *Symposium (International) on Combustion*, Vol. 18. Elsevier, 1981, pp. 175–185.

[8] R.L. Glick, *On statistical analysis of composite solid propellant combustion*, AIAA Journal 12 (1974), pp. 384–385.

[9] M. Shusser, F.E. C. Culick, and N.S. Cohen, *Analytical solution for pressure-coupled combustion response functions of composite solid propellants*, Journal of Propulsion and Power 24 (2008), pp. 1058–1067.

[10] J.A. Spurling, *Modeling Effects of Initial Temperatures on a Propellant's Pressure-Coupled Response Using a Pseudo Propellant Model*, in *50th AIAA/ASME/SAE/ASEE Joint Propulsion Conference*. 2014, p. 3494.

[11] N.S. Cohen, *Review of composite propellant burn rate modeling*, AIAA Journal 18 (1980), pp. 277–293.

[12] M.L. Gross and M.W. Beckstead, *Diffusion flame calculations for composite propellants predicting particle-size effects*, Combustion and Flame 157 (2010), pp. 864–873.

[13] T. Jackson and J. Buckmaster, *Heterogeneous propellant combustion*, AIAA journal 40 (2002), pp. 1122–1130.

[14] J. Buckmaster, T. Jackson, L. Massa, and M. Ulrich, *Response of a burning heterogeneous propellant to small pressure disturbances*, Proceedings of the Combustion Institute 30 (2005), pp. 2079–2086.

[15] S. Varunkumar, M. Zaved, and H.S. Mukunda, *A novel approach to composite propellant combustion modeling with a new heterogeneous quasi one-dimensional (HeQu1-D) framework*, Combustion and Flame (2016).

[16] M. Zaved, *Steady heterogeneous quasi 1-D model for AP-HTPB based composite propellants*, Master's thesis, Indian Institute of Technology, Madras, 2017, Available at `https://home.iitm.ac.in/varuns/Thesis_Zaved_2017.pdf`.

[17] S. Varunkumar and H. Mukunda, *Aluminized composite propellant combustion modeling with heterogeneous quasi-one dimensional (HeQu1-D) approach*, Combustion and Flame 192 (2018), pp. 59–70.

[18] F.S. Blomshield, C. Bicker, and R.A. Stalnaker, *High pressure pulsed motor firing combustion instability investigations*, in *1997 AIAA Joint Propulsion Meeting, Paper*. 97-3253, 1997.

[19] V. Wadhai and S. Varunkumar, *Linear instability and DC shift in tactical missile solid rocket motors – a computational study*, in *11^{th} ASPACC, The University of Sydney, NSW Australia*. 2017.

[20] W. Vishal, *Unsteady Heterogeneous Quasi 1D Model for AP/HTPB based Composite Propellants*, Master's thesis, Indian Institute of Technology, Madras, 2016, Available at `https://home.iitm.ac.in/varuns/thesis_vishal.pdf`.

[21] T. Mitani and T. Niioka, *Double flame structure in AP combustion*, in *Symposium (International) on Combustion*, Vol. 20. Elsevier, 1985, pp. 2043–2049.

[22] G. Lengelle, J. Duterque, and J. Trubert, *Physico-chemical mechanisms of solid pro-*

pellant combustion, Solid propellant chemistry, combustion, and motor interior ballistics(A 00-36332 09-28), Reston, VA, American Institute of Aeronautics and Astronautics, Inc.(Progress in Astronautics and Aeronautics. 185 (2000), pp. 287–334.

[23] R.R. Miller, *Effects of particle size on reduced smoke propellant ballistics*, AIAA paper 1096 (1982).

[24] M. Ibiricu, *Experimental studies on the oscillatory combustion of solid propellants*, Naval Weapons Center (1969).

Appendix

Estimation of A_c and ϕ_c

Quantities A_c and ϕ are obtained by solution of the unsteady heat conduction equation for the condensed phase given in Eqn. 1.

$$\frac{\partial T}{\partial t} + \dot{r}\frac{\partial T}{\partial x} = \alpha \frac{\partial^2 T}{\partial x^2} \tag{1}$$

where, α is the thermal diffusivity of condensed phase taken to be constant and equal to 0.1 mm^2/s. Boundary and initial conditions are given in Equations 2 and 3.

$$x \to -\infty,\ T \to T_0; \quad x = 0,\ T = T_s = \bar{T_s}(1 + \epsilon_T sin(2\pi f t)) \tag{2}$$

$$t = 0, \quad \frac{T(x) - T_0}{\bar{T_s} - T_0} = exp\left(\frac{\bar{\dot{r}}x}{\alpha}\right) \tag{3}$$

Numerical integration is required to solve Equation 1; for this purpose, the semi-infinite domain is mapped to a finite domain using the transformation given in Equation 4 along with other non-dimensional variables.

$$\zeta = exp\left(\frac{x\bar{\dot{r}}}{\alpha}\right); \quad \tau = \frac{t\bar{\dot{r}}^2}{\alpha}; \quad f_s = \frac{f\alpha}{\bar{\dot{r}}^2}; \quad \theta = \frac{T}{\bar{T_0}}; \quad R = \frac{\dot{r}}{\bar{\dot{r}}} \tag{4}$$

The transformed conduction equation is given by Equation 5.

$$\frac{\partial \theta}{\partial \tau} = \zeta^2 \frac{\partial^2 \theta}{\partial \zeta^2} + (1 - R)\zeta \frac{\partial \theta}{\partial \zeta} \tag{5}$$

Corresponding boundary and initial conditions are given in Equations 6 and 7.

$$\zeta = 0,\ \theta = \theta_0 = 1; \quad \zeta = 1,\ \theta = \theta_s = \frac{\bar{T_s}}{T_0}(1 + \epsilon_T sin(2\pi f_s \tau)) \tag{6}$$

$$\tau = 0, \quad \frac{\theta(\zeta) - \theta_0}{1 - \theta_0} = \zeta \tag{7}$$

Flux amplification factor, A_c is the ratio of the amplitude of fluctuations in condensed phase heat flux to the amplitude of imposed fluctuations in the surface temperature

of the propellant (ϵ_T), and angle, ϕ_c is a phase difference between heat flux fluctuations and surface temperature fluctuations. A_c and ϕ_c as a function of frequency are obtained by solving transformed unsteady diffusion equation (Equation 5) with boundary conditions given in Equations 6 and 7.

Crank-Nicholson implicit scheme for time and second order central differencing for space are used to discretise Equation 5 which results in a tridiagonal system of equations. For an imposed surface temperature fluctuation of a given frequency, the resultant tridiagonal system of equations are solved using TDMA solver to obtain time evolution of temperature profile in the condensed phase. Condensed phase heat flux as a function of time is calculated from the gradient of the obtained temperature profile as $q_c = k[\Delta T/\Delta x]_{x=0}$. Variation in temperature profile in condensed phase with time for 1% fluctuation in surface temperature is shown in Figure 1. Imposed surface temperature fluctuations are having mean of 994 K and frequency of 250 Hz. Figure 2 shows percentage fluctuations in condensed phase heat along with surface temperature fluctuations for the case discussed above.

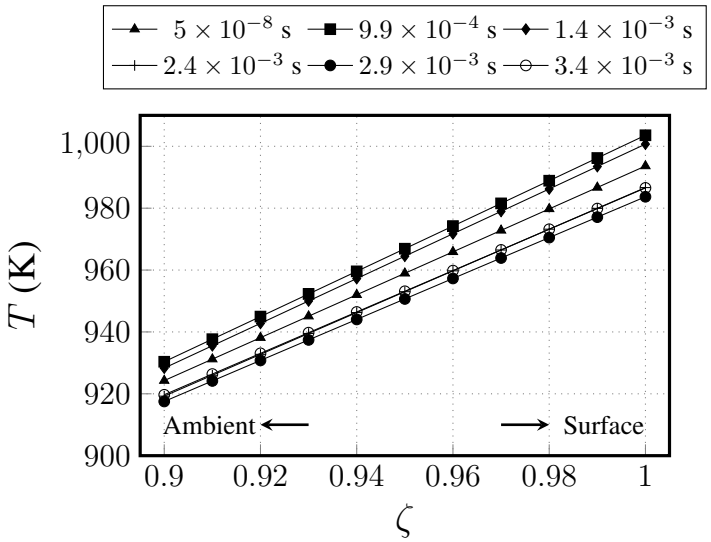

Figure 1. Time evolution of temperature profile in condensed phase for 1% fluctuation in surface temperature at 250 Hz.

For a given frequency, the flux amplification factor (A_c) and phase difference (ϕ_c) are obtained from Equation 8, respectively. For the case shown in Figure 2, A_c and ϕ_c are calculated as 5.3 and -0.08 rad, respectively.

$$A_c = \frac{|q_c'/\bar{q}_c|}{\epsilon_T}; \quad \phi_c = cos^{-1}\left(\frac{< q_c', T_s' >}{\sqrt{< q_c', q_c' >< T_s', T_s' >}}\right) \tag{8}$$

Crank-Nicholson scheme used here to discretise Equation 5 is unconditionally stable, but the accuracy of the solution was found to be affected by the size of grid and time steps, particularly at higher frequencies. Grid and time step independence studies were carried out to fix grid size and time step. Analysis carried out for grid and time step independence is shown in Figure 3, where A_c and ϕ_c are calculated against non-dimensional frequency f_s. The imposed surface temperature boundary condition is same as shown in Figure 2. For grid independence (Figure 3a), A_c and ϕ_c are calculated

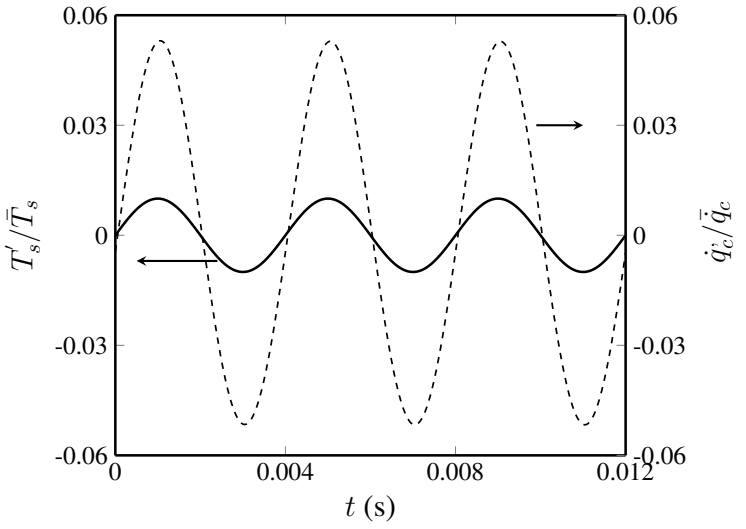

Figure 2. Fluctuations in condensed phase heat flux for 1% fluctuation in surface temperature at 250 Hz.

for $\Delta\zeta$ of 0.1, 0.02, 0.01 and 0.002 using $\Delta\tau$ of $3.6e-5$. The solution is found to be independent for $\Delta\zeta$ less than or equal to 0.01.

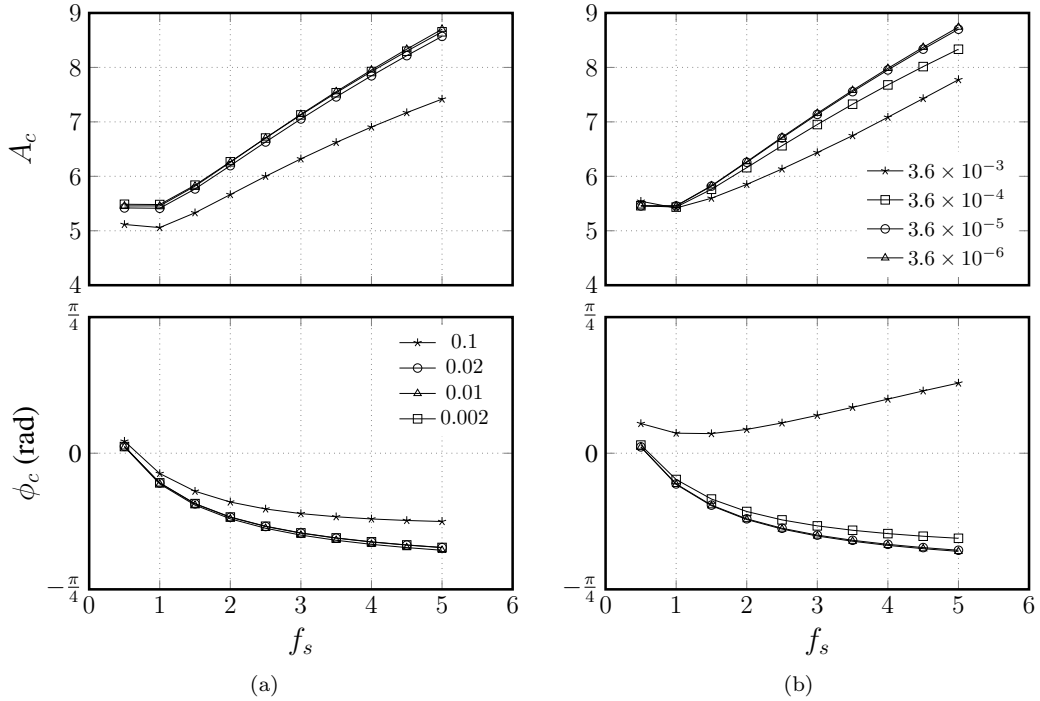

Figure 3. A_c and ϕ_c variation with f_s presented for (a) grid independence study (b) time step independence study.

Figure 3b shows results from time step independence study, where A_c and ϕ_c are calculated for $\Delta\tau$ of $3.6e-3$, $3.6e-4$, $3.6e-5$ and $3.6e-6$ with $\Delta\zeta$ of 0.01. The solution seems to be time independent below non-dimensional time step ($\Delta\tau$) of 3.6e-4 at all frequencies. For a given non-dimensional time step ($\Delta\tau$), $\Delta t = \Delta\tau\,\bar{r}^2/\alpha$ varies with

particle size. Heterogeneous propellants contain particles with burn rate ranging from order of one to ten mm/s giving rise to different dimensional time steps (Δt). Instead, it is preferred to use a fixed minimum Δt which will give a value of $\Delta\tau$ less than $1e-4$. With this constraint, dimensional time step for all computations to calculate frequency response was chosen to be $5e-8$ s.